

## Article

# Impact Features Induced by Single Fast Ions of Different Charge-State on Muscovite Mica

Igor Alencar <sup>1,2</sup> , Marcos R. Silva <sup>2</sup>, Rafael Leal <sup>2</sup>, Pedro L. Grande <sup>3</sup>  and Ricardo M. Papaléo <sup>2,\*</sup> 

<sup>1</sup> Departamento de Física, Universidade Federal de Santa Catarina (UFSC), Florianópolis CEP 88040-900, Santa Catarina, Brazil; igor.alencar@ufsc.br

<sup>2</sup> Escola Politécnica, Pontifícia Universidade Católica do Rio Grande do Sul (PUCRS), Porto Alegre CEP 90619-900, Rio Grande do Sul, Brazil; nanomarcos.silva@gmail.com (M.R.S.); rafael.leal@jeol.com.br (R.L.)

<sup>3</sup> Instituto de Física, Universidade Federal do Rio Grande do Sul (UFRGS), Porto Alegre CEP 91501-970, Rio Grande do Sul, Brazil; grande@if.ufrgs.br

\* Correspondence: Papaleo@pucrs.br; Tel.: +55-51-3320-3682

**Abstract:** The influence of the charge state  $q$  on surface modifications induced by the impact of individual fast, heavy ions on muscovite mica was investigated. Beams of 593 MeV  $^{197}\text{Au}^{q+}$  with well-defined initial charge states over a relatively broad range of values (30 to 51) and at different irradiation geometries were used. At normal incidence, the impact features are rounded protrusions (hillocks) with  $\gtrsim 20$  nm in diameter. At grazing angles, besides the hillocks, craters and elongated tails (up to 350 nm-long) extending along the direction of ion penetration are produced. It is shown that the impact features at normal incidence depend strongly on the initial charge state of the projectiles. This dependence is very weak at grazing angles as the ion reaches the equilibrium charge state closer to the surface. At normal ion incidence, the hillock volume scales with  $q^{3.3 \pm 0.6}$ . This dependence stems largely from the increase in the hillock height, as a weak dependence of the diameter was observed.

**Keywords:** ion track; surface modification; single ion impact; charge state; mica; electronic stopping power; scanning force microscopy



**Citation:** Alencar, I.; Silva, M.R.; Leal, R.; Grande, P.L.; Papaléo, R.M. Impact Features Induced by Single Fast Ions of Different Charge-State on Muscovite Mica. *Atoms* **2021**, *9*, 17. <https://doi.org/10.3390/atoms9010017>

Received: 12 January 2021  
Accepted: 19 February 2021  
Published: 25 February 2021

**Publisher's Note:** MDPI stays neutral with regard to jurisdictional claims in published maps and institutional affiliations.



**Copyright:** © 2021 by the authors. Licensee MDPI, Basel, Switzerland. This article is an open access article distributed under the terms and conditions of the Creative Commons Attribution (CC BY) license (<https://creativecommons.org/licenses/by/4.0/>).

## 1. Introduction

Modification of materials by localized and dense electronic excitations produced by fast ions, electron, or laser beams is the basis of various structuring tools used in an increasing number of applications. The amount of energy pumped to the electronic system may be very high, triggering, if its relaxation is sufficiently slow, substantial atomic motion and particle ejection at the surface [1,2]. In particular, for individual fast heavy ions, a trail of modified material is produced along the material (the latent track), which can subsequently be developed into pores of different shapes [3]. At the surface, nanometer-sized craters or protrusions may be directly produced as a result of an ion impact, modifying locally its topography and its physico-chemical structure [4–8]. Patterning of surfaces for nanofabrication of devices [9,10] is one of the most prominent applications.

Cratering or hillock formation is observed for ions in a broad energy range: in the so-called nuclear regime (kinetic energies around tens of keV), where ballistic collisions dominate [4,11]; for slow highly-charged ions, where potential energy transfer to the target dominates [12]; or for ions with energies in excess of  $\sim 0.1$  MeV/u where energy deposition occurs mainly via electronic excitation [6,8,13–15]. Depending on the energy regime of the ions and the type of material being bombarded, the shape of the impact features and the underlying mechanisms of formation may differ, but the resultant structures are always huge compared to the atomic size of the particles that produce them. For example, in metals, a 400 keV Au ion impacting on a thin Au layer can produce rimmed craters containing thousands of atoms [16]; in polymers, a 200 MeV Au ion is able to eject, at grazing angles,

a volume of material corresponding to a mass of  $\sim 10^6$  u [17]; in ionic crystals, a 180 MeV Au ion may eject a nanoparticle with a diameter of  $\gtrsim 10$  nm [18].

In this work, we focus on surface modification in muscovite mica induced by high velocity ions with non-equilibrium charge-states in the electronic stopping regime. For a 3 MeV/u Au ion, more than 99% of the energy lost by the ions is deposited in the electronic subsystem. A considerable fraction (50% or more) of the energy deposited in the track of a swift heavy ion is concentrated in a core region of  $\sim 1$  nm radius, where ionizations are directly produced by the ions. The emitted secondary electrons spread the rest of the energy over larger areas. The exact dimension of such regions (i.e., the excitation volume) depends on the velocity of the ions. Due to the high energy density in the core of the impact, melting or even evaporation may occur [19]. The sudden expansion of the material in the core may also generate pressure waves [20,21], which, together with the thermal effects, are believed to be the major sources for cratering and mass transport. The exact mechanism underlying the topological changes induced by fast ion impacts is, however, not well-understood. Comparison between theory and experiments may be further obscured by thermomechanical relaxation effects of the surface features, which may occur long after the thermalization of the ion track region [22].

When swift heavy ions travel in a material with an initial charge state  $q$  different from its equilibrium value, charge exchange processes occur until the charge reaches a steady-state value  $q_{eq}$ . Usually the equilibration length is short, but for sufficiently fast ions (e.g., 3 MeV/u Au), it can be hundreds of nanometers, a figure comparable or much larger than thin layers present in a great number of devices. As the stopping power,  $dE/dx$ , depends nonlinearly on  $q$  (typically  $dE/dx \propto q^n$ , with  $n < 2$  [23]), near-surface effects of ion-solid interactions (such as surface tracks) may depend strongly on  $q$ . Indeed, we have demonstrated that this is the case for crater features in polymeric thin films [15]. The exact dependence of the size of impact features on  $q$  is thickness dependent, but here we show that, even for surfaces of bulk materials, the  $q$  effects are still important. We also explore the variation of  $q$  with penetration depth to estimate the size of the excited region below the surface that contributes to crater and hillock formation.

Muscovite mica is an insulating, layered crystalline silicate with high radiation sensitivity and, consequently, it is frequently employed as an external, passive particle detector [24]. Cleavage produces atomically flat surfaces ideally smooth for studying surface modification induced by ion irradiation with Scanning Force Microscopy (SFM). For these reasons, radiation effects at mica surfaces had been comprehensively investigated with a variety of scanning modes in the literature [13,25–35]. It is important to note that cross-sectional diameters obtained via SFM are systematically higher than other techniques such as Transmission Electron Microscopy (TEM) [36] or Small-Angle X-ray Scattering (SAXS) [37,38]. This apparent discrepancy had been attributed to the sensitivity of the technique employed to detect the amorphous track immersed in a diluted crystalline phase [37]. By comparing topographic and phase-contrast modes, we give further support to this hypothesis. Additionally, charge-state effects in mica had only been reported for slow highly charged ions [39–45]. The charge state of fast ions may contribute significantly to the electronic stopping power at the surface [46]. For instance, it had been demonstrated to influence crater formation in polymeric thin films [15] and electronic sputtering in ionic crystals [47].

## 2. Results

### 2.1. Electronic Stopping Power at the Surface

The charge-state dependent electronic stopping power was calculated using the approach of Schiwietz and Grande [48] provided in the program CasP6.0. The calculations gave a parameterization of the electronic stopping power for mica in the form of  $(dE/dx)_{el} \propto q^{1.21}$  (Figure 1). The calculated electronic stopping power  $(dE/dx)_{el}$  varied from 2000 eV/Å ( $q = 30$ ) up to 3700 eV/Å ( $q = 51$ ). At the equilibrium charge state, the CasP6.0 values are in good agreement with the SRIM code estimations [49].

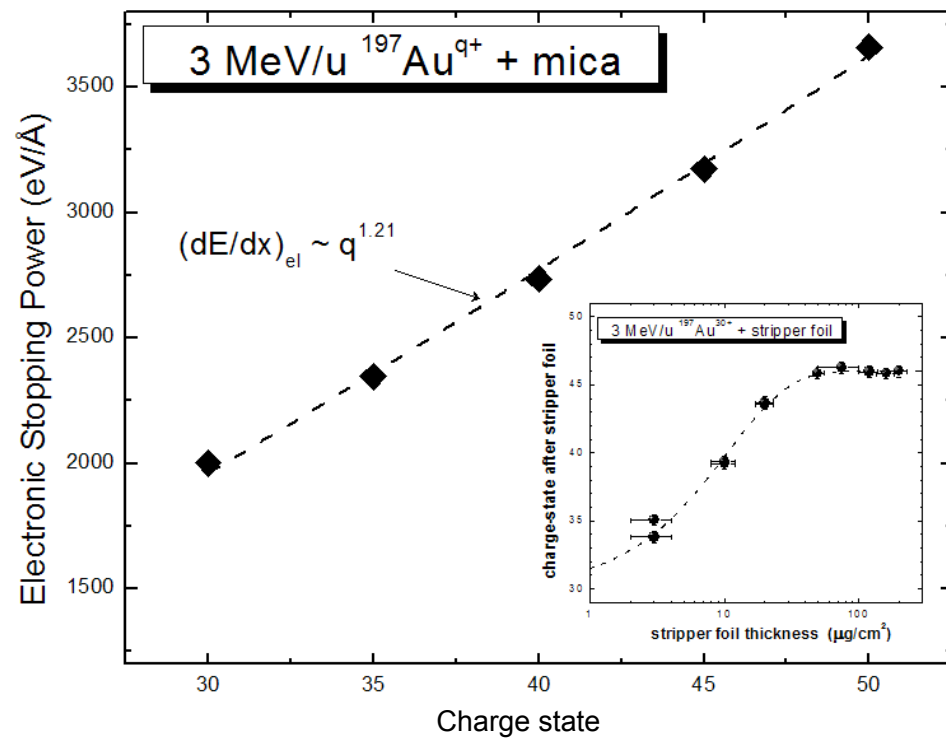


**Figure 1.** Electronic stopping power for 593 MeV Au beams of different charge states  $q$  in mica as calculated by the code CasP6.0. These Au charge states are obtained from 593 MeV Au<sup>30+</sup> ions exiting amorphous carbon foils of different thicknesses (see inset with data from Grande et al. [50]). Well-defined initial charge states reach the targets, as the beam passes through a series of magnetic analysers in the way to the irradiation chamber.

The equilibrium charge-state obtained in amorphous carbon films (see Materials and Methods section) was  $q_{\text{eq}} = 46.3 \pm 0.1$  and shall also hold for mica, as it is weakly dependent on the atomic number of the target. Because of the high atomic number and speed of the 3 MeV/u Au ion, it has a large charge equilibration distance within the target. The half equilibration-depth estimated for mica is  $l_{\text{eq}} \sim 40$  nm (again, see Materials and Methods section). In addition, because the projectile velocities are the same, the size of the excitation volume near the surface (determined by the range of secondary electrons) is fixed for all  $q$ , and the mean deposited energy density in the ion tracks  $\varepsilon$  is simply proportional to  $(dE/dx)_{\text{el}}$ . That is,  $dE/dx$  scalings can be obtained free from distortions which may arise when beams of different velocities are used.

## 2.2. Phase Imaging and the Nature of the Impact Features

Figure 2a,b show topographic and phase images of surface modifications produced by 3 MeV/u Au<sup>51+</sup> ions impinging at normal incidence on mica. The impact features at normal incidence appear only as protrusions. At grazing incidence (Figure 2c,d), very small craters and extremely long tails (with lengths that can reach 350 nm or more) are seen. Such tails tend to broaden at the end and have a height of only a few atomic planes but are still clearly visible on the flat mica surfaces. The images also clearly show shallow elliptical craters. Craters on mica have not been observed in previous works with atomic ions (only when C<sub>60</sub> cluster beams in the MeV range were used [31]). This difference in observation is, most probably, a tip effect, and demonstrates the improved quality (smaller tip radius) of the tips used in the present work.

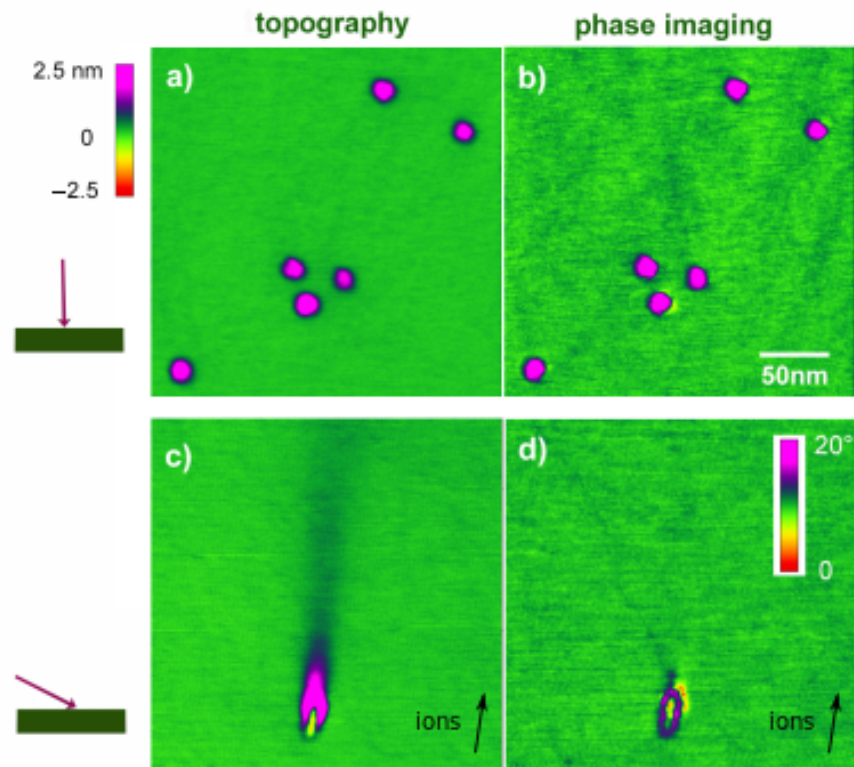
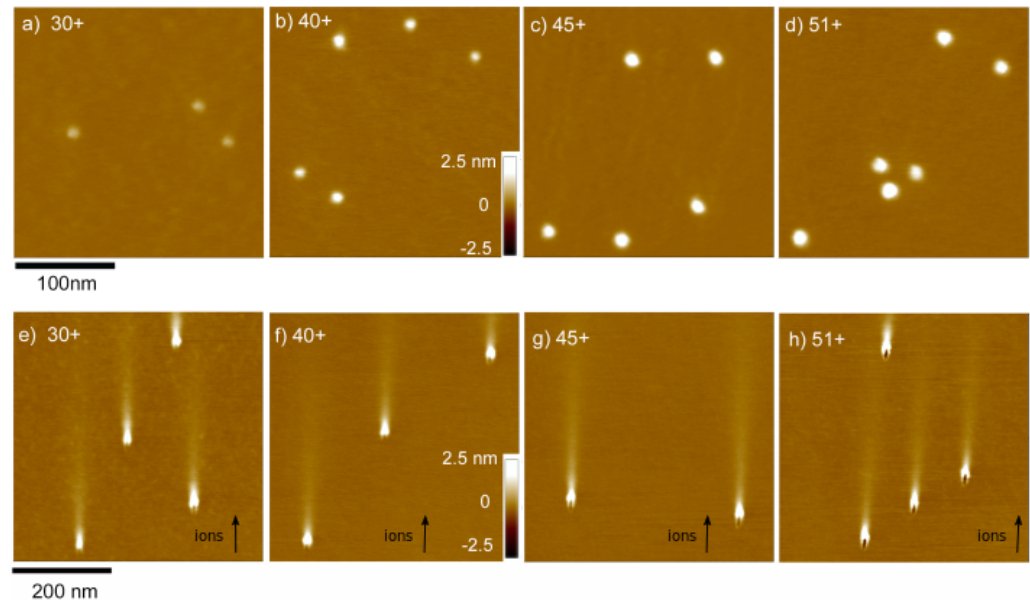


**Figure 2.** Topographic (a,c) and phase (b,d) SFM images of individual ion tracks produced by 3 MeV/u Au<sup>51+</sup> ions on freshly-cleaved mica surfaces. The scale bar of 50 nm applies to all images. The color scale covers variations of height of  $\pm 2.5$  nm relative to the unmodified surface in the topographic channels and phase shifts of  $20^\circ$  in the phase images. Black arrows indicate the direction of the ion beam for grazing incidence.

Images of phase contrast, a mode usually not explored in radiation damage studies, provide additional information about the impact features. The phase contrast emerges basically from changes in energy dissipation between the oscillating SFM tip and the sample. It has been used to detect local changes in composition [51], but the contrast could also be induced by changes in curvature at the boundaries of topographic features. Hillocks observed on mica present a (positive) phase shift, both at normal and grazing incidence. At normal incidence, the region where the phase shift is seen correlates very well with the lateral size of the protruded volume. This indicates that hillocks are not only the result of a physical expansion of the the material but might as well involve some sort of chemical modification. However, at grazing angles, only part of the protruded region surrounding the crater (and the crater area itself) has a phase shift. The long tail shows no phase contrast and behaves much like pristine mica, suggesting that, in this case, only a gentle physical displacement of atoms is involved. It has been shown previously by high-resolution imaging that tails in mica have preserved crystal lattice [26], whilst at the center of the impact a softer and disordered structure is formed, with enlarged friction [25]. Taken together, the present results and previous observations give support to the idea that the raised regions produced by the ion impact, at distances sufficiently away from the impact center, are a volume of material dislodged from their position by a gentle mechanical process, involving little structural modification. On the other hand, the amorphised central hillock in mica, which are close to the center of the transiently heated ion track, where the deposited energy density is highest, underwent substantial rearrangement.

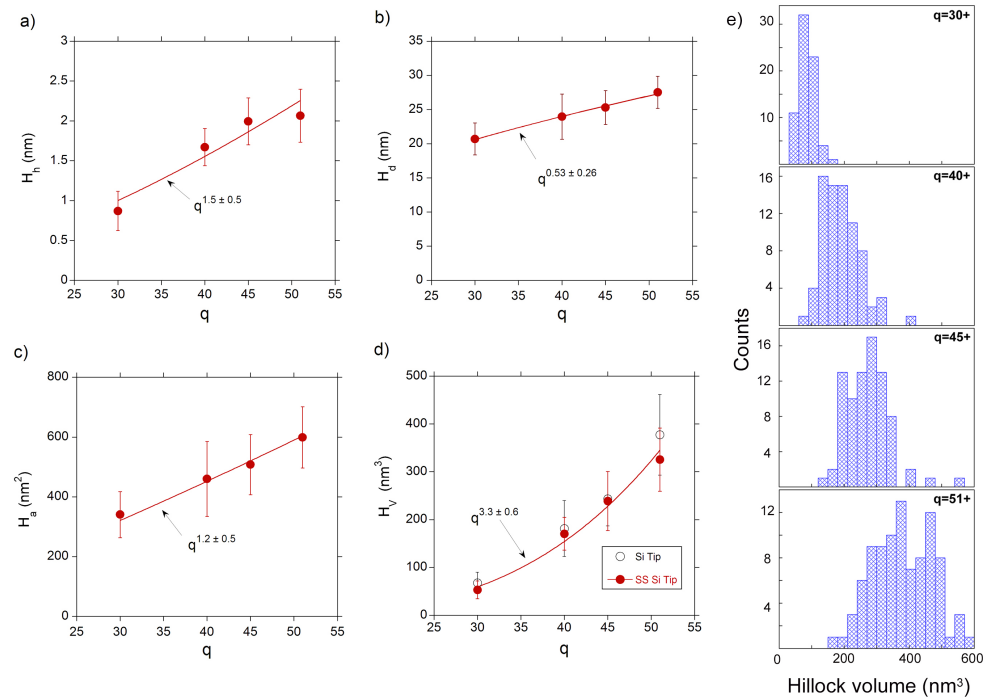
### 2.3. Impact Features Induced by Ions of Different Initial Charge States $q$

Figure 3 shows typical images of impact features produced by 3 MeV/u Au of different initial charge states in mica at normal and grazing incidence ( $11^\circ$  to the surface). A clear correlation of the size of hillocks with the charge state is seen at normal incidence, but this effect disappears for glancing collisions. Only the crater size appears to be slightly affected by the charge state at grazing angles.



**Figure 3.** SFM images of mica crystals bombarded at two different angles of incidence by 3 MeV/u Au <sup>$q+$</sup>  of different initial charge states. Images (a–d) depict impacts at normal incidence and images (e–h) are of samples bombarded at grazing incidence ( $11^\circ$  to the surface). The entrance charge state is given in each panel. The color (height) scale is the same for all images. The scale bar of 100 nm applies to images (a–d), and the bar of 200 nm to images (e–h). Black arrows indicate the direction of the ion beam for grazing incidence.

Figure 4 depicts the average hillock dimensions as a function of  $q$  for irradiations at normal incidence. Each data point is a mean value over about 50–100 impact features. The bars are not actually error bars, but a measure of the fluctuations in size of the individual surface tracks because of the statistical nature of the energy deposition by each individual ion. The fluctuations in the hillock volume are relatively large (up to  $\sim 30\%$ ), considering the high  $(dE/dx)_{el}$  of 3 MeV/u Au and are not the result of mixing data from tips of distinct sharpness. In order to evaluate possible effects of the tip quality on the scaling of the hillock size with  $q$ , we have also plotted separately mean values calculated from two sets of tips: the standard Si tips (with nominal apex radii better than 10 nm) and the supersharp Si tips (with nominal radii below 2 nm). Apart from the obvious enlargement of hillock size when standard tips are used, no significant differences in the  $q$  dependence were seen. At grazing incidence, the dimensions are independent of the charge state (data not shown).



**Figure 4.** Average dimensions of hillocks induced in mica by projectiles of different initial charge state impinging at normal incidence: (a) height  $H_h$ ; (b) diameter  $H_d$ ; (c) area  $H_a$ ; and (d) volume  $H_v$ . Solid lines depict the scaling of each dimension with  $q$ , fitted to power laws. The influence of using tips of different sharpnesses is also illustrated for the hillock volume; (e) histograms showing the distribution of hillock volumes for the different initial charge states.

### 3. Discussion

#### 3.1. Scaling of Surface Tracks with the Initial Charge State

For normal incidence, hillock volume in mica scales as  $q^{3.3 \pm 0.6}$  (Figure 4d). This dependence stems largely from the increase in the hillock height ( $\propto q^{1.5 \pm 0.5}$ ), as a much weaker dependence of the diameter was observed ( $\propto q^{0.53 \pm 0.26}$ ). The scaling for the hillock volume is similar to the dependence found for rim volumes produced by the same 3 MeV/u Au ions in 105 nm-thick PMMA films (also a cubic dependence), but weaker than the  $q^{5.5 \pm 0.10}$  observed in 10 nm-thick PMMA films [15]. That is, excitation at deep layers in mica at which the charge state has changed towards equilibrium also contributes to hillock formation. Near-surface events (at depths smaller than the half-equilibration length of  $\sim 40$  nm) still provide the largest fraction of the energy and momentum needed. On the other hand, in the case of grazing angles (Figure 3e–h), the  $q$ -state effects completely vanish. This is expected because of the larger path traversed by the ions inside the material to reach a given depth (a factor of 5 longer compared to normal incidence) and the closer proximity to the surface of regions excited under a charge-state equilibrium condition. Thus, when the path length is comparable to or larger than the half-equilibration depth the charge state of the fast ion,  $q$  do vary towards the same (equilibrium) charge state and, consequently, the  $q$ -effects smear out because the effective charge state in the material will be close to this equilibrium value ( $q_{eq} = 46.3 \pm 0.1$ ), irrespective of the initial, entrance charge-states. This is, of course, the situation reported in this work. Data from such bulk-like conditions at least show qualitatively how important the near surface is to the formation of the surface tracks. We also note that the fitting exponents found in the scaling relations are not strongly affected ( $<10\%$ , i.e., smaller than the reported uncertainties) by the inclusion of a threshold formation of hillocks ( $350 \text{ eV}/\text{\AA}$ ) [52].

Ignoring the smoothing effect of the deeply excited layers on the  $q$ -dependence, and using the relation  $(dE/dx)_{el} \propto q^{1.21}$  shown in Figure 1, the  $(dE/dx)_{el}$  dependence of

hillock volume extracted from the normal incidence data is  $H_V \propto (dE/dx)_{el}^{2.73}$ . Applying the same procedure to the hillock diameter, one gets  $H_d \propto (dE/dx)_{el}^{0.44}$ . The hillock diameter has been used in the past to deduce ion track sizes and compare to measurements extracted from TEM or SAXS. In our view, such comparisons must be taken with care, as hillock creation is a phenomenon influenced by material expansion and flow near the free surface. Such relaxation phenomena coupled to the well-known tip convolution effects of SFM often make the size of surface tracks larger than those extracted from the aforementioned techniques [6]. We note that the present results for the hillock diameter, even when supersharp tips were used, are systematically higher than those reported previously for the same electronic stopping power using SFM. However, the deduced  $dE/dx$  dependence for the hillock diameter in our work is similar to previous results found in the literature [6,34].

Although it is hard to evaluate the “true” size of the features imaged by SFM, it is possible to estimate to what extent the scalings of the impact features with  $q$  may be distorted by the size and geometry of the SFM tip. In a first approximation, the measured feature is a convolution of the true size and the detector response which is fixed and determined by the tip radius. Thus, the finite size of the tip will affect much more the small protrusions at the lower  $q$ -state than the large ones. Therefore, the finite tip size would make the scalings with  $q$  less steep. This means that the power laws presented here are a lower limit to the actual values. Experimentally, we observe only a slight increase in the exponent of the power law of the protruded volumes with  $q$  ( $\sim 10\%$ ) when the supersharp tips were used in comparison with the standard tips, well within the uncertainties of the fittings (Figure 4d).

Finally, we add a few notes on the increase in size dispersion at larger  $q$ . This effect is quite large and a bit surprising, as size fluctuations supposedly correlate with fluctuations in the local deposited energy, which should be smaller than the total deposited energy itself for increasing values of  $q$ . In fact, for any value of  $q$ , the energy-loss straggling is dominated by close collisions events and thus it will depend mostly on nuclear charge of projectile  $Z$ . Therefore, the energy-loss straggling for a fixed  $q$  will be given by the Bohr straggling formula at high projectile energies. However, since the projectile charge, and hence the stopping power, fluctuates during its slowing down, an extra energy-loss straggling mechanism comes into play. This so-called charge–exchange straggling can exceed the Bohr value by 1–2 orders of magnitude for heavy ions in the MeV/u energy regime [53] and therefore could explain the present experimental results.

## 4. Materials and Methods

### 4.1. Targets and Bombardment Conditions

The heavy-ion cyclotron at the Hahn–Meitner Institute (Berlin, Germany) was used to produce beams of 3 MeV/u  $^{197}\text{Au}^{q+}$  (593 MeV) with well-defined charge states  $q$  over a relatively broad range of  $q$  values. Initially, a careful check of the intensity of possible beams was performed, using carbon foils of various thicknesses (from 3 to 200  $\mu\text{g}/\text{cm}^2$ ), placed after the acceleration stage. For a beam of 593 MeV  $\text{Au}^{30+}$  exiting the cyclotron, a range of charge states from 30 to 51 was achievable. In this way, the mean exit charge-state  $q_{\text{mean}}$  was obtained as a function of the thickness of the carbon foils. This allowed the extraction of the equilibrium charge-state ( $q_{\text{eq}} = 46.3 \pm 0.1$ ) and the equilibration depth in amorphous carbon (a-C). The half equilibration-depth for a-C is  $\sim 50$  nm (Figure 1, inset). For mica, the equivalent half equilibration-depth is  $l_{\text{eq}} \sim 40$  nm (obtained by simple scaling of the mass densities).

Specimens of muscovite mica ( $\rho = 2.83$  g/cm<sup>3</sup>) were cleaved immediately before loading them into the irradiation chamber. They were bombarded in vacuum ( $\sim 2 \times 10^{-6}$  Torr) with scanned 3 MeV/u  $\text{Au}^{q+}$  beams ( $q = 30, 40, 45, \text{ and } 51$ ) at two distinct angles of incidence ( $0^\circ$  and  $79^\circ$  to the surface normal). The impact density was around  $\sim 10$  ions/ $\mu\text{m}^2$ , controlled by a charge integration system.

#### 4.2. SFM Measurements

The size and shape of the surface tracks were characterized offline with a Nanoscope IIIa (Digital Instruments Inc., Tonawonda, NY, USA) scanning probe microscope in the intermittent contact mode at ambient conditions. Only images collected with high quality Si tips were stored and used for quantitative evaluation of the data. Special care was taken for using the same tip (or at least tips of similar quality) to image the set of samples covering the complete range of charge states. We made no effort to implement offline corrections aiming to deconvolute tip-shape effects on the measured dimensions. However, the effect of using probes of different tip radii was checked by comparing images (and quantitative data derived from such images) obtained with standard Si tips (Budget Sensors, Innovative Solutions Bulgaria Ltd., Sofia, Bulgaria) with super sharp tips (Applied NanoStructures Inc., Mountain View, CA, USA) that have, nominally, a factor of four smaller tip radius ( $\sim 2$  nm). A detailed discussion of the influence of the tip on the metrology of surface tracks can be found elsewhere [7].

All measurements of impact features were performed considering the root mean square (RMS) roughness of the pristine mica surfaces  $h_{\text{pristine}}$  (0.05 nm) as the reference height level. The  $h_{\text{pristine}}$  values were used to define the lateral sizes of the impact features as well as the height of the reference plane needed in the hillock area and volume determination. The area and volume of the hillocks were obtained directly by the image analysis software, thus no assumptions were made regarding the shape of the impact features to extract such data. The reference plane was rectangular, with a size sufficient to encompass each individual impact feature. For impacts at normal incidence, the size of the plane was  $60 \times 60$  nm<sup>2</sup>. For grazing angles, it was  $300 \times 100$  nm<sup>2</sup>. During the measurements, the reference plane was initially positioned at the hillocks and afterwards translated to neighbor areas in order to also measure the volume of the local roughness. Three to four points around the hillocks were sampled. The effective volumes were taken as the difference between the hillock volume and the volume due to pure roughness in the selected region. For each charge state, a minimum of 50 impacts were analyzed to extract the mean values of the surface tracks dimensions.

#### 5. Conclusions

The impact features induced on mica surfaces by 3 MeV/u Au individual heavy ions with well-defined initial charge states and normal incidence depend strongly on the projectile charge state  $q$ . Under such conditions, the volume of the hillocks was found to increase as  $q^{3.3 \pm 0.6}$ , which correspond to an electronic stopping power dependence  $H_V \propto (dE/dx)_{\text{el}}^{2.73}$ . For the hillock diameter, on the other hand,  $H_d \propto (dE/dx)_{\text{el}}^{0.44}$ , close to the scaling deduced for the track diameter in mica crystals using TEM and SAXS. For grazing angles of incidence, the  $q$ -dependence of hillocks is very weak as the ions reach the equilibrium charge state closer to the surface. Tiny craters were also observed at grazing incidence especially at the largest  $q$ , implying that processes leading to craters are more surface sensitive than those that result in the production of protrusions.

**Author Contributions:** Conceptualization, P.L.G. and R.M.P.; methodology, P.L.G. and R.M.P.; software, P.L.G.; formal analysis, M.R.S., R.L., and R.M.P.; writing—original draft preparation, I.A. and R.M.P.; writing—review and editing, I.A., P.L.G., and R.M.P.; supervision, R.M.P.; funding acquisition, P.L.G. and R.M.P. All authors have read and agreed to the published version of the manuscript.

**Funding:** This research was funded by DAAD (Germany) and by Brazilian agencies CAPES (finance code 001), FAPERGS, and CNPq. This research was also developed under the auspices of the National Institute of Science and Technology (INCT) for Surface Engineering (contract 465423/2014-0) and PRONEX-FAPERGS (contract 16/2551-0000479-0).

**Data Availability Statement:** The data presented in this study are available on request from the corresponding author.

**Acknowledgments:** The authors are grateful to Gregor Schiwietz (Helmholtz-Zentrum Berlin, Germany) for the assistance during the irradiations and for insightful discussions.

**Conflicts of Interest:** The authors declare no conflict of interest. The funders had no role in the design of the study; in the collection, analyses, or interpretation of data; in the writing of the manuscript, or in the decision to publish the results.

### Abbreviations

The following abbreviations are used in this manuscript:

a-C	amorphous carbon
RMS	root mean square
SAXS	small-angle X-ray scattering
SFM	scanning force microscopy
TEM	transmission electron microscopy

### References

- Fleischer, R.L.; Price, P.B.; Walker, R.M. *Nuclear Tracks in Solids—Principles and Applications*; University of California Press: Berkeley, CA, USA, 1975; p. 626.
- Spohr, R. *Ion Tracks and Microtechnology: Principles and Applications*; Vieweg: Braunschweig, Germany, 1990; p. 282.
- Lang, M.; Glasmacher, U.A.; Moine, B.; Neumann, R.; Wagner, G.A. Etch-pit morphology of tracks caused by swift heavy ions in natural dark mica. *Nucl. Instr. Methods B* **2004**, *218*, 466–471. [[CrossRef](#)]
- Donnelly, S.E.; Birtcher, R.C. Heavy ion cratering of gold. *Phys. Rev. B* **1997**, *56*, 13599–13602. [[CrossRef](#)]
- Eriksson, J.; Rottler, J.; Reimann, C.T. Fast-ion-induced surface tracks in bioorganic films. *Int. J. Mass Spectrom. Ion Proc.* **1998**, *175*, 293–308. [[CrossRef](#)]
- Neumann, R. Scanning probe microscopy of ion-irradiated materials. *Nucl. Instr. Meth. B* **1999**, *151*, 42–55. [[CrossRef](#)]
- Papaléo, R.M. Surface tracks and cratering in polymers. In *Fundamentals of Ion-Irradiated Polymers*; Fink, D., Ed.; Springer-Verlag: Heidelberg, Germany, 2004; pp. 207–250.
- Akcöltekin, E.; Peters, T.; Meyer, R.; Duvenbeck, A.; Klusmann, M.; Monnet, I.; Lebius, H.; Schleberger, M. Creation of multiple nanodots by single ions. *Nat. Nanotechnol.* **2007**, *2*, 290–294. [[CrossRef](#)]
- Watt, F.; Bettiol, A.A.; van Kan, J.A.; Teo, E.J.; Breese, M.B.H. Ion beam lithography and nanofabrication: A review. *Int. J. Nanosci.* **2005**, *4*, 269–286. [[CrossRef](#)]
- Bruchhaus, L.; Marazov, P.; Bischoff, L.; Gierak, J.; Wieck, A.D.; Hövel, H. Comparison of technologies for nano device prototyping with a special focus on ion beams: A review. *Appl. Phys. Rev.* **2017**, *4*, 011302. [[CrossRef](#)]
- Samela, J.; Nordlund, K.; Popok, V.N.; Campbell, E.B. Origin of complex impact craters on native oxide coated silicon surfaces. *Phys. Rev. B* **2008**, *77*, 075309. [[CrossRef](#)]
- El-Said, A.S.; Heller, R.; Meissl, W.; Ritter, R.; Facsko, S.; Lemell, C.; Solleder, B.; Gebeshuber, I.C.; Betz, G.; Toulemonde, M.; et al. Creation of nanohillocks on CaF<sub>2</sub> surfaces by single slow highly charged ions. *Phys. Rev. Lett.* **2008**, *100*, 237601. [[CrossRef](#)]
- Thibaudau, F.; Cousty, J.; Balanzat, E.; Bouffard, S. Atomic-force-microscopy observations of tracks induced by swift Kr ions in mica. *Phys. Rev. Lett.* **1991**, *67*, 1582–1585. [[CrossRef](#)]
- Kopniczky, J.; Reimann, C.T.; Hallén, A.; Sundqvist, B.U.R.; Tengvall, P.; Erlandsson, R. Scanning-force-microscopy study of MeV-atomic-ion-induced surface tracks in organic crystals. *Phys. Rev. B* **1994**, *49*, 625–628. [[CrossRef](#)]
- Papaléo, R.M.; Silva, M.R.; Leal, R.; Grande, P.L.; Roth, M.; Schattat, B.; Schiwietz, G. Direct evidence for projectile charge-state dependent crater formation due to fast ions. *Phys. Rev. Lett.* **2008**, *101*, 167601. [[CrossRef](#)] [[PubMed](#)]
- Birtcher, R.C.; Donnelly, S.E.; Schlutig, S. Nanoparticle ejection from Au induced by single Xe ion impacts. *Phys. Rev. Lett.* **2000**, *85*, 4968–4971. [[CrossRef](#)]
- Farenzena, L.S.; Livi, R.P.; Araújo, M.A.; Bermudez, G.G.; Papaléo, R.M. Cratering and plastic deformation in polystyrene induced by MeV heavy ions: Dependence on the molecular weight. *Phys. Rev. B* **2001**, *63*, 104108. [[CrossRef](#)]
- Alencar, I.; Hatori, M.; Marmitt, G.G.; Trombini, H.; Grande, P.L.; Dias, J.F.; Papaléo, R.M.; Mücklich, A.; Assmann, W.; Toulemonde, M.; et al. Nanoparticle emission by electronic sputtering of CaF<sub>2</sub> single crystals. *Appl. Surf. Sci.* **2021**, *537*, 147821. [[CrossRef](#)]
- Toulemonde, M.; Benyagoub, A.; Trautmann, C.; Khalifaoui, N.; Boccanfuso, M.; Dufour, C.; Gourbilleau, F.; Grob, J.J.; Stoquert, J.P.; Costantini, J.M.; et al. Dense and nanometric excitations induced by swift heavy ions in an ionic CaF<sub>2</sub> crystal: Evidence for two thresholds of damage creation. *Phys. Rev. B* **2012**, *85*, 054112. [[CrossRef](#)]
- Johnson, R.E.; Sundqvist, B.U.R.; Hedin, A.; Fenyö, D. Sputtering by fast ions based on a sum of impulses. *Phys. Rev. B* **1989**, *40*, 49–53. [[CrossRef](#)]
- Klaumünzer, S. Thermal-spike models for ion track physics: A critical examination. *Mat. Fys. Meddelelser* **2006**, *52*, 293–328.
- Papaléo, R.M.; Leal, R.; Carreira, W.H.; Barbosa, L.G.; Bello, I.; Bulla, A. Relaxation times of nanoscale deformations on the surface of a polymer thin film near and below the glass transition. *Phys. Rev. B* **2006**, *74*, 094203. [[CrossRef](#)]
- Grande, P.L.; Schiwietz, G. Impact-parameter dependence of the electronic energy loss of fast ions. *Phys. Rev. A* **1998**, *58*, 3796–3801. [[CrossRef](#)]

24. Jonckheere, R. On the densities of etchable fission tracks in a mineral and co-irradiated external detector with reference to fission-track dating of minerals. *Chem. Geol.* **2003**, *200*, 41–58. [[CrossRef](#)]
25. Hagen, T.; Grafström, S.; Ackermann, J.; Neumann, R.; Trautmann, C.; Vetter, J.; Angert, N. Friction force microscopy of heavy-ion irradiated mica. *J. Vacuum Sci. Technol. B* **1994**, *12*, 1555–1558. [[CrossRef](#)]
26. Barlo Daya, D.D.N.; Hallén, A.; Hakansson, P.; Sundqvist, B.U.R.; Reimann, C.T. Scanning force microscopy study of surface tracks induced in mica by 78.2-MeV <sup>127</sup>I ions. *Nucl. Instr. Methods B* **1995**, *103*, 454–465. [[CrossRef](#)]
27. Barlo Daya, D.D.N.; Hallén, A.; Eriksson, J.; Kopniczky, J.; Papaléo, R.M.; Reimann, C.T.; Hakansson, P.; Sundqvist, B.U.R.; Brunelle, A.; Della-Negra, S.; et al. Radiation damage features on mica and L-valine probed by scanning force microscopy. *Nucl. Instr. Methods B* **1995**, *106*, 38–42. [[CrossRef](#)]
28. Ackermann, J.; Angert, N.; Neumann, R.; Trautmann, C.; Dischner, M.; Hagen, T.; Sedlacek, M. Ion track diameters in mica studied with scanning force microscopy. *Nucl. Instr. Methods B* **1996**, *107*, 181–184. [[CrossRef](#)]
29. Barlo Daya, D.D.N.; Reimann, C.T.; Hallén, A.; Sundqvist, B.U.R.; Hakansson, P. Latent (sub-surface) tracks in mica studied by tapping mode scanning force microscopy. *Nucl. Instr. Methods B* **1996**, *111*, 87–90. [[CrossRef](#)]
30. Neumann, R.; Ackermann, J.; Angert, N.; Trautmann, C.; Sedlacek, M. Ion tracks in mica studied with scanning force microscopy using force modulation. *Nucl. Instr. Methods B* **1996**, *116*, 492–495. [[CrossRef](#)]
31. Barlo Daya, D.D.N.; Reimann, C.T.; Hakansson, P.; Sundqvist, B.U.R.; Brunelle, A.; Della-Negra, S.; Le Beyec, Y. Crater formation due to grazing incidence C<sub>60</sub> cluster ion impacts on mica: A tapping-mode scanning force microscopy study. *Nucl. Instr. Methods B* **1997**, *124*, 484–489. [[CrossRef](#)]
32. Ackermann, J.; Müller, A.; Neumann, R.; Wang, Y. Scanning force microscopy on heavy-ion tracks in muscovite mica: Track diameter versus energy loss and loading force. *Appl. Phys. A* **1998**, *66*, 1151–1154. [[CrossRef](#)]
33. Vorobyova, I.; Reimann, C.; Toulemonde, M. Comparison of the structure and sizes of tracks induced by high-energy monatomic and cluster ions incident on the surface of mica. *Nucl. Instr. Methods B* **2000**, *166–167*, 959–963. [[CrossRef](#)]
34. Bouffard, S.; Leroy, C.; Della-Negra, S.; Brunelle, A.; Costantini, J.M. Damage production yield by electron excitation in mica for ion and cluster irradiations. *Philos. Mag. A* **2001**, *81*, 2841–2854. [[CrossRef](#)]
35. Gruber, E.; Bergen, L.; Salou, P.; Lattouf, E.; Grygiel, C.; Wang, Y.; Benyagoub, A.; Levavasseur, D.; Rangama, J.; Lebius, H.; et al. High resolution AFM studies of irradiated mica: Following the traces of swift heavy ions under grazing incidence. *J. Phys. Condens. Matter* **2018**, *30*, 285001. [[CrossRef](#)]
36. Vetter, J.; Scholz, R.; Dobrev, D.; Nistor, L. HREM investigation of latent tracks in GeS and mica induced by high energy ions. *Nucl. Instr. Methods B* **1998**, *141*, 747–752. [[CrossRef](#)]
37. Chailley, V.; Dooryhee, E.; Bouffard, S.; Balanzat, E.; Levalois, M. Observations by X-ray diffraction of structural changes in mica irradiated by swift heavy ions. *Nucl. Instr. Methods B* **1994**, *91*, 162–167. [[CrossRef](#)]
38. Chailley, V.; Dooryhee, E.; Levalois, M. Amorphization of mica through the formation of GeV heavy ion tracks. *Nucl. Instr. Methods B* **1996**, *107*, 199–203. [[CrossRef](#)]
39. Schneider, D.; Briere, M.A.; Clark, M.W.; McDonald, J.; Biersack, J.; Siekhaus, W. Atomic displacement due to the electrostatic potential energy of very highly charged ions at solid surfaces. *Surf. Sci.* **1993**, *294*, 403–408. [[CrossRef](#)]
40. Schneider, D.; Briere, M.A.; McDonald, J.; Biersack, J. Ion/surface interaction studies with 1–3 keV/amu ions up to Th<sup>80+</sup>. *Radiat. Eff. Defects Solids* **1993**, *127*, 113–136. [[CrossRef](#)]
41. Parks, D.C.; Bastasz, R.; Schmieder, R.W.; Stöckli, M. Nanometer-size surface features produced by single, low energy, highly charged ions. *J. Vacuum Sci. Technol. B* **1995**, *13*, 941–948. [[CrossRef](#)]
42. Ruehlicke, C.; Briere, M.; Schneider, D. AFM studies of a new type of radiation defect on mica surfaces caused by highly charged ion impact. *Nucl. Instr. Methods B* **1995**, *99*, 528–531. [[CrossRef](#)]
43. Parks, D.C.; Stöckli, M.P.; Bell, E.W.; Ratliff, L.P.; Schmieder, R.W.; Serpa, F.G.; Gillaspay, J.D. Non-kinetic damage on insulating materials by highly charged ion bombardment. *Nucl. Instr. Methods B* **1998**, *134*, 46–52. [[CrossRef](#)]
44. Ritter, R.; Kowarik, G.; Meissl, W.; El-Said, A.S.; Maunoury, L.; Lebius, H.; Dufour, C.; Toulemonde, M.; Aumayr, F. Nanostructure formation due to impact of highly charged ions on mica. *Vacuum* **2010**, *84*, 1062–1065. [[CrossRef](#)]
45. Wang, Y.; Zhao, Y.; Sun, J.; Wang, Z.; Liu, J.; Li, J.; Xiao, G. Creation of nanodots on mica surfaces induced by highly charged xenon ions. *Nucl. Instr. Methods B* **2012**, *286*, 299–302. [[CrossRef](#)]
46. Toulemonde, M. Irradiation by swift heavy ions: Influence of the non-equilibrium projectile charge state for near surface experiments. *Nucl. Instr. Methods B* **2006**, *250*, 263–268. [[CrossRef](#)]
47. Assmann, W.; Ban-d’Etat, B.; Bender, M.; Boduch, P.; Grande, P.L.; Lebius, H.; Lelièvre, D.; Marmitt, G.G.; Rothard, H.; Seidl, T.; Severin, D.; Voss, K.O.; Toulemonde, M.; Trautmann, C. Charge-state related effects in sputtering of LiF by swift heavy ions. *Nucl. Instr. Methods B* **2017**, *392*, 94–101. [[CrossRef](#)]
48. Schiwietz, G.; Grande, P.L. Improved charge-state formulas. *Nucl. Instr. Methods B* **2001**, *175–177*, 125–131. [[CrossRef](#)]
49. Ziegler, J.F.; Ziegler, M.D.; Biersack, J.P. SRIM – The stopping and range of ions in matter (2010). *Nucl. Instr. Methods B* **2010**, *268*, 1818–1823. [[CrossRef](#)]
50. Grande, P.L.; Nagamine, L.C.C.M.; Morais, J.; Alves, M.C.M.; Schiwietz, G.; Roth, M.; Schattat, B.; Baggio-Saitovitch, E. High-energy ion beam irradiation of Co/NiFe/Co/Cu multilayers: Effects on the structural, transport and magnetic properties. *Thin Solid Films* **2008**, *516*, 2087–2093. [[CrossRef](#)]

- 
51. Scott, W.W.; Bhushan, B. Use of phase imaging in atomic force microscopy for measurement of viscoelastic contrast in polymer nanocomposites and molecularly thick lubricant films. *Ultramicroscopy* **2003**, *97*, 151–169. [[CrossRef](#)]
  52. Szenes, G. General features of latent track formation in magnetic insulators irradiated with swift heavy ions. *Phys. Rev. B* **1995**, *51*, 8026–8029. [[CrossRef](#)]
  53. Sigmund, P.; Osmani, O.; Schinner, A. Anatomy of charge-exchange straggling. *Nucl. Instr. Methods B* **2014**, *338*, 101–107. [[CrossRef](#)]